Inorganic Chemistry

Article

pubs.acs.org/IC

Crystal Structures of $Li_6B_4O_9$ and $Li_3B_{11}O_{18}$ and Application of the Dimensional Reduction Formalism to Lithium Borates

Gwenaëlle Rousse,*[†,‡] Benoît Baptiste,[†] and Gérald Lelong*[†]

[†]Institut de Minéralogie, de Physique des Matériaux, et de Cosmochimie (IMPMC), Sorbonne Universités-UPMC Univ Paris 06, UMR CNRS 7590, Muséum National d'Histoire Naturelle, IRD UMR 206, 4 Place Jussieu, F-75005 Paris, France

[‡]FRE 3677, Chimie du Solide et Energie, Collège de France, 11 Place Marcelin Berthelot, and Réseau sur le Stockage Electrochimique de l'Energie (RS2E), FR CNRS 3459, 75231 Paris Cedex 05, France

Supporting Information

ABSTRACT: The crystal structures of two members of the $Li_2O-B_2O_3$ phase diagram, $Li_6B_4O_9$ and $Li_3B_{11}O_{18}$, have been solved from single-crystal X-ray diffraction, and their structure has been further confirmed by Rietveld refinement on powder samples. $Li_6B_4O_9$ crystallizes in the $P2_1/n$ space group with a = 3.31913(15) Å, b = 23.361(2) Å, c = 9.1582(4) Å, and β = 92.650(4)°. It is the only lithium borate being built upon clusters made of four BO_3 triangular units linked by vertices. $Li_3B_{11}O_{18}$ adopts also a monoclinic symmetry with a = 17.7607(8) Å, b = 7.7737(4) Å, c = 9.6731(4) Å, and β = 100.906(4)° (space group $P2_1/c$); it contains 73% BO_3 triangular units and 27% BO_4 tetrahedra, linked by vertices such that it forms a 3D network containing B_3O_7 and B_5O_{10} rings. These two new structures and their specificities are discussed in the framework of the dimensional reduction formalism together with other reported lithium borates and may serve as a crystalline reference to study borate glasses.

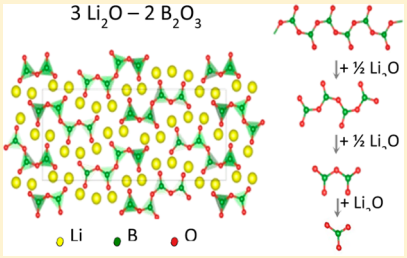

INTRODUCTION

The $Li_2O-B_2O_3$ binary diagram has been studied for more than 50 years and shows a great complexity (Figure 1).[1−5] About 10 single-phase compositions are reported in this diagram, some of them presenting also temperature- or pressure-induced polymorphism.[6] The structural diversity offered by borates is impressive, as boron oxides can be built upon triangular BO_3 units, tetrahedral BO_4 units, or both. The connectivity between these building units (denoted sometimes as "fundamental building blocks" or "superstructural units")[3,5] is also extremely diverse and may give rise to isolated units, dimers, chains, rings and so on.[5,7] Having a good knowledge of the structure and properties exhibited by the crystalline compounds may provide precious relevant information to serve as a reference for studying the properties of borate glasses, whose local structure is not so easily accessible. The most studied crystalline compound is LiB_3O_5 (Li_2O−3 B_2O_3)[8] because it can be used as a nonlinear optical material.[7,9] Some Li-rich phases such as Li_3BO_3 (3 $Li_2O-B_2O_3$)[10] present a good ionic conductivity, so that they could serve as solid electrolytes for Li-ion batteries.[11,12] As the BO_3 unit is lighter than other polyanions (phosphates, silicates, and sulfates), lithium borates including a 3d transition metal such as $LiFeBO_3$ are considered as promising Li-ion electrode materials.[13]

The structures of the crystalline compounds belonging to the $Li_2O-B_2O_3$ binary diagram have been explored over the last five decades, the most recent determination being the low- and high-temperature polymorphs of $Li_4B_2O_5$ (2 $Li_2O-B_2O_3$).[14] Despite many efforts, two compositions reported in the $Li_2O-B_2O_3$ diagram are still missing, as their structures could never be solved: $Li_6B_4O_9$ (3 Li_2O−2 B_2O_3) and $Li_2B_8O_{13}$ (Li_2O−4 B_2O_3). Indeed lithium borates are among the most difficult compounds to study from a crystallographic point of view, as they are made of light atoms, which are weak X-ray scatterers. When single crystals are not available, the usual successful way is to use neutron powder diffraction as a complementary technique to X-ray diffraction, but in the present case, such a study is quite challenging since natural boron, and to a lesser extent lithium, is one of the best neutron absorbers. This limitation can be circumvented by preparing ^{11}B- and ^{7}Li-doped compounds, but the limited variety and the cost of enriched precursors sometimes make the synthesis harder. Nevertheless, this strategy was successfully followed in the case of the Li-ion battery material $LiFeBO_3$[15,16] and in $Li_2B_4O_7$.[17]

In this paper, the structure resolution of $Li_6B_4O_9$ (3 Li_2O−2 B_2O_3) using single-crystal X-ray diffraction is reported, as well as that of $Li_2B_8O_{13}$ (Li_2O−4 B_2O_3), for which the reported composition was wrong and has to be read as $Li_3B_{11}O_{18}$ (3 Li_2O−11 B_2O_3). Rietveld refinements on powdered samples further confirm our structural models and indicate that the single-crystal structure is representative of the whole sample. These two structures are discussed in terms of topology and dimensional reduction formalism together with the other structures reported in the $Li_2O-B_2O_3$ phase diagram.

Received: February 13, 2014
Published: May 16, 2014

   dx.doi.org/10.1021/ic500331u | Inorg. Chem. 2014, 53, 6034−6041

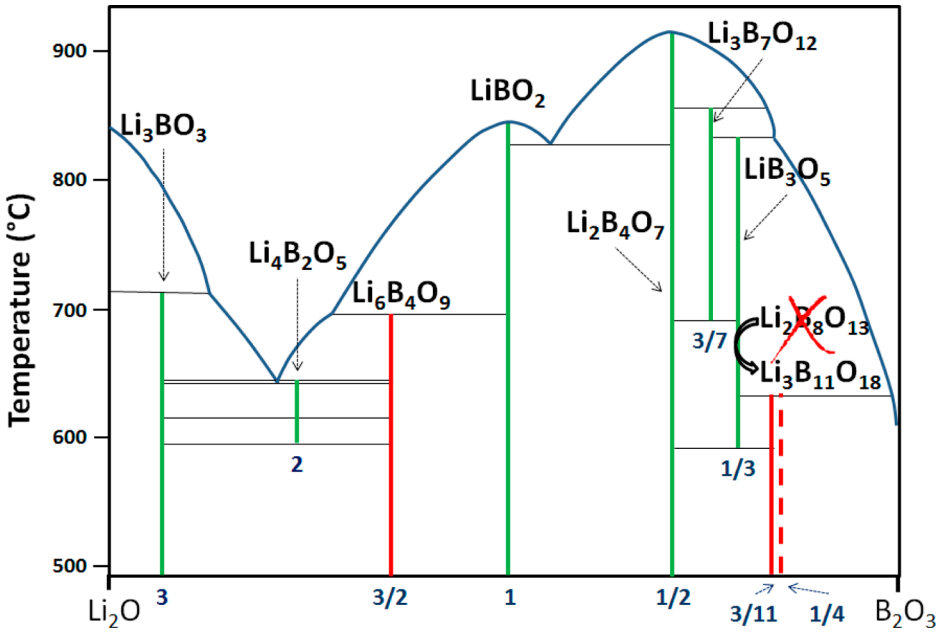

Figure 1. Binary phase diagram of Li_2O–B_2O_3, inspired from ref 2. The red and green vertical lines refer to single-phase compounds. Numbers refer to the Li_2O versus B_2O_3 ratio for each composition. The two red lines correspond to $Li_6B_4O_9$ and $Li_3B_{11}O_{18}$, which are the main subjects of this paper. $Li_3B_{11}O_{18}$ replaces the previously reported $Li_2B_8O_{13}$, which does not exist (shown therefore as a dashed red line).

EXPERIMENTAL METHODS

X-ray Diffraction. Single-crystal X-ray diffraction data for $Li_3B_{11}O_{18}$ and $Li_6B_4O_9$ were collected on an Oxford Diffraction Xcalibur-S diffractometer equipped with a Sapphire CCD-detector with Mo Kα radiation (λ = 0.71073 Å, graphite monochromator) at 293 K. Data reduction, cell refinement, space group determination, scaling, and empirical or analytical absorption correction[18] were performed using CrysAlisPro software.[19]

In both cases, the structures were solved through the Olex2 program[20] by direct methods using SHELXS-2013.[21] The refinement was then carried out with SHELXL-2013 by full-matrix least-squares minimization and difference Fourier methods. All atoms were refined with anisotropic displacement parameters.

A non-merohedric twinning was detected for the $Li_6B_4O_9$ crystal, giving rise to overlapped reflections. Two major components were identified (43% and 57%), and the indexed reflections for each lattice were integrated with the same unit cell parameters (the twin law is (1 0 0, 0 −1 0, −0.258 0 −1)). The structure was solved using only the reflections from the major domain with an overlapping factor less than 50%. The refinement was then carried out against the deconvoluted data sets of the two domains, decreasing the R_1 factor from 9.70% to 5.15%.

The X-ray powder diffraction (XRD) patterns were recorded using an X'Pert Pro Panalytical diffractometer equipped with either a Cu Kα radiation source ($\lambda_{K\alpha1}$ = 1.540 56 Å, $\lambda_{K\alpha2}$ = 1.544 39 Å) or a Co Kα radiation source ($\lambda_{K\alpha1}$ = 1.788 97 Å, $\lambda_{K\alpha2}$ = 1.792 85 Å) with an X'Celerator detector. Rietveld refinements[22] were performed with the FullProf suite of programs.[23] Vesta was used to visualize the crystal structures.[24]

RESULTS

Synthesis Approach and Structural Determination. a. $Li_6B_4O_9$. The $Li_6B_4O_9$ (3 Li_2O–2 B_2O_3) compound does not melt congruently (Figure 1); therefore a glass of the same composition was first prepared by mixing lithium carbonate (Li_2CO_3) and boric acid (H_3BO_3, reagent grade) in appropriate quantities and then melted at 950 °C for 15 min. Once melted, the sample was quenched, ground, and finally heated at 550 °C for 2 days with intermittent grindings, followed by a second heat treatment at 600 °C for about 2 days. This synthesis follows the protocol described by Mathews and co-workers.[25] The resulting X-ray powder diffraction pattern indicates the presence of numerous Bragg peaks, the first ones being seen at relatively low angle (2θ = 7.5° for λ_{Cu}), indicative of a large unit cell. Moreover, the strong overlapping of peaks at 2θ angles ranging between 26° and 31° suggests a low symmetry for the cell. This prevented finding a unique unit cell with indexing programs such as Dicvol,[26] as many large cells could account for the observed peak positions. Fortunately, the resulting $Li_6B_4O_9$ powder presents large agglomerates composed by several single crystals stacked together. By successive cuttings, a single crystal has been isolated with an approximate size of 260 × 150 × 110 μm^3, which is suitable for structure determination. The single-crystal X-ray diffraction data analysis leads to a monoclinic $P2_1/n$ cell with lattice parameters a = 3.31913(15) Å, b = 23.361(2) Å, c = 9.1582(4) Å, and β = 92.650(4)°. Note that the structure has not been normalized in the $P2_1/c$ setting, as this would lead to a β angle significantly different from 90°. Tables 1 and 2 gather the details for data collection and structure determination and the resulting atomic positions. (Anisotropic displacement parameters are given in the Supporting Information, Table S1.)

Four formula units per cell are found, and the lithium, boron, and oxygen atoms are distributed on the Wyckoff general position 4*e*, all with full occupancy. The four boron atoms are located in the middle of a regular triangle, forming planar BO_3 units, which are linked by vertices to form quasi-planar B_4O_9 groups made of four BO_3 (Figure 2a). These groups are oriented perpendicular to the [100] direction, forming a kind of lamellar structure composed of B_4O_9 platelet groups every $a/2$ (Figure 2b). Lithium atoms, which are located between these platelets, are coordinated only by oxygen atoms belonging to B_4O_9 groups. The Li–O distances range from 1.90 to 2.10 Å, with in addition a few longer Li–O bonds up to 2.40 Å, so that the lithium coordination varies from one to another. The six lithium atoms of the cell can be observed in distorted

dx.doi.org/10.1021/ic500331u | Inorg. Chem. 2014, 53, 6034–6041

Table 1. Measurements Conditions and Crystallographic Data for Room-Temperature Single-Crystal X-ray Diffraction on $Li_6B_4O_9$ and $Li_3B_{11}O_{18}$

parameter	$Li_6B_4O_9$	$Li_3B_{11}O_{18}$
fw/mg	228.88	427.73
temp/K	293	293
cryst syst	monoclinic	monoclinic
space group	$P2_1/n$	$P2_1/c$
a/Å	3.31913(15)	17.7607(8)
b/Å	23.361(2)	7.7737(4)
c/Å	9.1582(4)	9.6731(4)
α/deg	90.00	90.00
β/deg	92.650(4)	100.906(4)
γ/deg	90.00	90.00
volume/Å^3	709.35(8)	1311.42(10)
Z	4	4
ρ_{calc}/g·cm^{-3}	2.143	2.166
μ/mm^{-1}	0.188	0.203
F(000)	440.0	832
cryst size/μm^3	260 × 150 × 115	349 × 281 × 135
radiation	Mo Kα (λ = 0.71073 Å)	Mo Kα (λ = 0.71073 Å)
2θ range	6.98° to 52.74°	6.78° to 55.8°
reflns collected	2536	5710
indep reflns	1448	2864
	R_{int} = 0.029	R_{int} = 0.0341
	R_{sigma} = 0.021	R_{sigma} = 0.0477
data/restraints/params	1448/0/172	2864/0/289
goodness-of-fit on F^2	1.202	1.079
final R indexes = [$I > 2\sigma(I)$]	R_1 = 0.0515	R_1 = 0.0416
	wR_2 = 0.1265	wR_2 = 0.0951
final R indexes [all data]	R_1 = 0.0606	R_1 = 0.0595
	wR_2 = 0.1305	wR_2 = 0.1053
largest diff peak/hole/ e Å^{-3}	0.34/−0.30	0.30/−0.25

Table 2. Fractional Atomic Coordinates (×10^4) and Equivalent Isotropic Displacement Parameters (Å^2 × 10^3) for $Li_6B_4O_9$

atom	x	y	z	U(eq)[a]
Li1	6909(10)	6186.9(16)	3198(4)	24.0(8)
Li2	−1805(10)	4425.5(14)	9588(3)	19.0(7)
Li3	−2405(9)	4580.0(14)	5094(3)	17.3(6)
Li4	−3213(10)	6434.4(14)	10217(4)	18.9(7)
Li5	1675(10)	7040.2(13)	8502(3)	17.2(7)
Li6	1836(10)	7059.0(13)	3035(3)	15.9(6)
B1	2583(6)	4770.3(9)	7622(2)	12.3(4)
B2	1742(6)	5863.5(9)	7971(2)	13.8(4)
B3	1956(6)	6479.8(8)	5639(2)	13.2(4)
B4	1732(6)	7568.0(9)	5827(2)	12.3(4)
O1	2764(4)	4740.1(5)	6175.9(13)	14.3(3)
O2	3099(4)	4314.4(5)	8537.8(13)	14.8(3)
O3	1624(4)	5287.0(5)	8369.3(14)	18.8(3)
O4	1619(4)	6243.3(5)	9044.7(13)	13.9(3)
O5	2033(4)	5980.7(5)	6504.2(14)	20.1(3)
O6	1678(4)	6993.2(5)	6381.6(14)	18.1(3)
O7	2098(4)	6403.3(5)	4218.5(13)	14.1(3)
O8	1676(4)	7977.5(5)	6876.1(14)	15.4(3)
O9	1810(4)	7679.1(5)	4397.1(13)	14.7(3)

[a] U_{eq} is defined as 1/3 of the trace of the orthogonalized U_{ij} tensor.

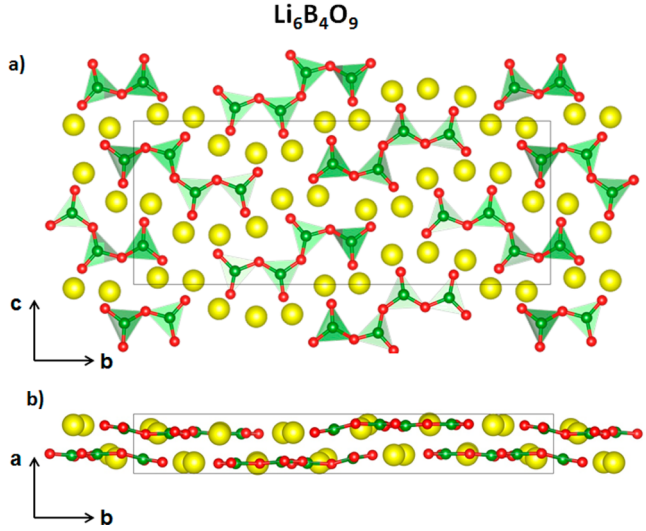

Figure 2. Structure of $Li_6B_4O_9$, viewed along [100] (a) and [001] (b). B, O, and Li atoms are colored green, red, and yellow, respectively; BO_3 triangular units are colored green.

tetrahedra and in trigonal bypiramids (see the Supporting Information, Figure S1). In addition, Li−O and B−O distances and calculated bond valence sums using the Zachariasen formula $V_i = \sum_j s_{ij} = \sum_j e^{(d_0-d_{ij})/0.37}$ using the parameters d_0, characterizing a cation−anion pair, taken from ref 27 for Li, B, and O are in good agreement with the expected valences of +1, +3, and −2 (see the Supporting Information, Table S2).

Using the shorthand notation[5] that defines the building units composed of BO_3 triangles (Δ) and BO_4 tetrahedra (T), $Li_6B_4O_9$ can be written as 4:[(1:4Δ)].

A Rietveld refinement was then attempted on the powder diffraction pattern, to check if the single crystal was representative of the powder synthesized at the same composition. The refinement was carried out starting from the model in Table 2, and only B and O atomic positions were refined first. An overall displacement parameter was imposed that is the same for each chemical species. As the refinement converged rapidly, we further refined the Li positions, which happen to be stable, indicating that the structure determined from single-crystal diffraction perfectly fits the powder pattern. Since the peak width was larger than the instrumental one, isotropic size parameters (inducing a fwhm varying as $Y/\cos\theta$) and strain parameters were refined. The isotropic strain X can be decoupled from the size parameters Y because it varies as $X \tan\theta$. The average crystallite size was refined to 431(2) Å. Anisotropic strain parameters, whose S_{hkl} values using Stephens notation[28] are reported in Table 3 together with the lattice parameters obtained from powder, indicate some fluctuations of lattice parameters along the [100] direction, while they are at

Table 3. Results of the Rietveld Refinement on the X-ray Powder Pattern of $Li_6B_4O_9$

	$Li_6B_4O_9$, X-ray diffractometer, λ_{Cu}	
$P2_1/n$		R_{Bragg} = 1.73%
a = 3.33413(8) Å	c = 9.1860(3) Å	V = 717.12(3) Å^3
b = 23.4388(5) Å	β = 92.6143(16) deg	
Strain Parameters		
S_{400} = 19.0(9), S_{040} = 0.0027(3), S_{004} = 0.23(2), S_{220} = 1.12(7), S_{202} = 6.8(6)		
S_{022} = 0.028(8), S_{121} = −0.12(5), S_{301} = 5.6(6), S_{103} = 1.7(2)		

dx.doi.org/10.1021/ic500331u | Inorg. Chem. 2014, 53, 6034−6041

the smallest along [010]. This comes as no surprise, considering that the rigidity of the structure comes from the way BO_3 units are arranged: the BO_3 triangles are linked through vertices in the [010] direction (this direction therefore involves covalent bonds), while the B_4O_9 platelets are stacked along [100]; therefore in this direction, only Li atoms make the connection between them via ionic bonds, enhancing the flexibility. The final Rietveld refinement of $Li_6B_4O_9$ is shown in Figure 3.

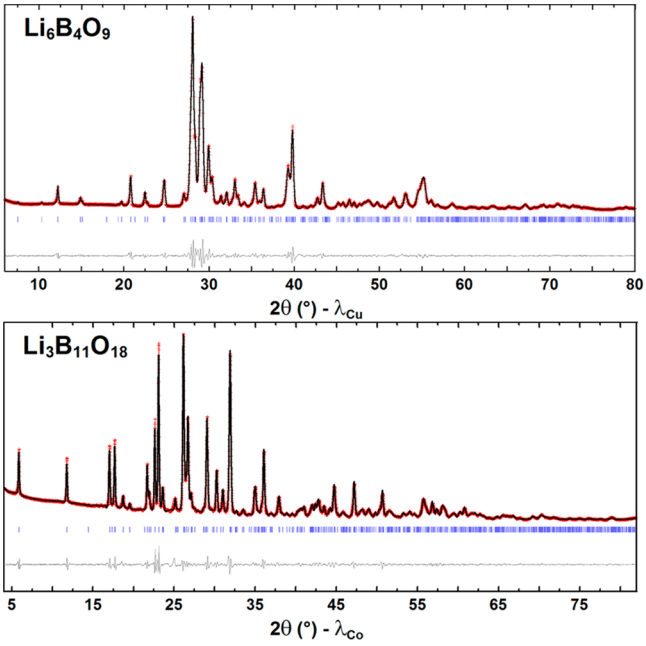

Figure 3. Rietveld refinement of the $Li_6B_4O_9$ X-ray powder diffraction pattern (λ_{Cu}) (top) and $Li_3B_{11}O_{18}$ X-ray powder diffraction pattern (λ_{Co}) (bottom). For both, the red crosses are the experimental points, the black line is the calculated pattern, blue vertical tick marks refer to Bragg reflections, and the gray line is the difference (observed − calculated) pattern.

b. $Li_3B_{11}O_{18}$ (Previously Reported as $Li_2B_8O_{13}$). The same strategy was followed for the reported composition $Li_2B_8O_{13}$, for which a unit cell was reported by Touboul et al.,[11] but the poor quality of their single crystals prevented them from obtaining a structural model. Another group reported a triclinic unit cell to index the pattern but could not provide any structural model.[25,29] This comes as no surprise, as we figured out that the composition was wrong as shown later. As for $Li_6B_4O_9$, the synthesis procedure of $Li_2B_8O_{13}$ followed the protocol described by Mathews et al.[25] Lithium carbonate (Li_2CO_3) and boric acid (H_3BO_3, reagent grade) were melted at 950 °C for 30 min, and the resulting powder was quenched, ground, and finally reheated at 550 °C for 2 days with intermittent grindings, followed by a second heat treatment at 600 °C for 24 h. The "$Li_2B_8O_{13}$" powder indeed shows a plethora of peaks with a strong overlap, and the first diffraction peak located at the large value of d = 17.4 Å precluded us from easily finding a unique unit cell able to index the pattern. As for $Li_6B_4O_9$, a single crystal of sufficient quality was isolated within the powder to perform single-crystal X-ray diffraction. Details on the data acquisition can be found in Table 1. Importantly, the structure solution led to the unit formula $Li_3B_{11}O_{18}$, i.e., 3 Li_2O−11 B_2O_3, instead of the $Li_2B_8O_{13}$ (Li_2O−4 B_2O_3) expected. $Li_3B_{11}O_{18}$ crystallizes in the $P2_1/c$ space group with lattice parameters a = 17.7607(8) Å, b = 7.7737(4) Å, c = 9.6731(4) Å, and β = 100.906(4)°. The lithium, boron, and oxygen atoms are distributed in the general 4*e* Wyckoff site (see Table 4 for the complete list of atomic positions). The anisotropic temperature factors are gathered in the Supporting Information, Table S3. There are three lithium, 11 boron, and 18 oxygen atoms in the structure. Two distinct kinds of boron coordination are observed: eight boron atoms are located in the middle of a regular BO_3 triangle, whereas three boron atoms are in the middle of BO_4 regular tetrahedra. These BO_3 and BO_4 units are linked only with vertices, so as to form a 3D interconnected network (Figure 4). Each BO_4 tetrahedron is linked to two corner-sharing BO_3 triangles, so as to form almost planar $B^{[4]}$−O−$B^{[3]}$−O−$B^{[3]}$−O−$B^{[4]}$ six-membered rings (the value written between square brackets indicates the coordination of boron), creating B_3O_7 rings (Figure 4c). All boron atoms are involved in such units. There are two crystallographically distinct B_3O_7 building units, plus one that is more specific as the BO_4 tetrahedron connects two B_3O_7 rings that are perpendicular to each other to form B_5O_{10} bi-rings (Figure 4c). The shorthand notation[5] of $Li_3B_{11}O_{18}$ can be written as $8{:}\infty^3[(3{:}2\Delta{+}T){+}(5{:}4\Delta{+}T)]$, where Δ and T refer to a BO_3 triangle and a BO_4 tetrahedron, respectively.

Table 4. Fractional Atomic Coordinates (×10⁴) and Equivalent Isotropic Displacement Parameters (Å² × 10³) for $Li_3B_{11}O_{18}$

atom	*x*	*y*	*z*	*U*(eq)[a]
Li1	9555(3)	−3191(7)	9896(4)	45.4(13)
Li2	7536(2)	−802(8)	7787(4)	41.2(13)
Li3	5789(2)	5605(7)	6342(4)	39.7(11)
B1	9926.2(14)	1311(3)	7475(2)	19.3(5)
B2	9044.2(14)	826(3)	9032(2)	20.1(5)
B3	8063.6(14)	−1164(4)	5094(2)	19.6(5)
B4	7125.1(14)	1042(4)	4901(2)	20.4(5)
B5	6246.9(14)	1588(3)	6541(2)	20.4(5)
B6	5135.9(14)	2110(3)	7523(2)	19.5(5)
B7	3070.2(14)	4397(3)	4649(2)	20.3(5)
B8	1828.4(14)	5674(4)	4268(2)	21.3(5)
B9	9121.7(14)	−1262(3)	7192(2)	18.3(5)
B10	4130.5(14)	4413(3)	6860(2)	19.3(5)
B11	2417.6(14)	5110(4)	2216(2)	22.1(6)
O1	9572.5(8)	−2636(2)	7991.9(14)	20.2(3)
O2	9631.7(8)	−25(2)	6648.7(14)	22.5(4)
O3	8694.6(8)	−410(2)	8138.2(13)	19.8(3)
O4	9710.8(8)	1597(2)	8776.4(14)	23.1(4)
O5	8651.5(8)	−2004(2)	5937.2(14)	20.9(3)
O6	7553.1(8)	−221(2)	5720.0(14)	25.0(4)
O7	6617.9(9)	2017(2)	5471.7(14)	24.2(4)
O8	6413.1(8)	143(2)	7317.1(14)	19.6(3)
O9	7572.0(8)	−124(2)	9816.9(13)	20.9(4)
O10	5646.8(8)	2668(2)	6694.3(15)	24.9(4)
O11	5268.2(8)	641(2)	8282.6(15)	23.0(4)
O12	4473.0(8)	2888(2)	7598.6(15)	24.1(4)
O13	3740.4(8)	3934(2)	5449.8(14)	24.4(4)
O14	3035.7(9)	4305(2)	3235.5(14)	25.7(4)
O15	2775.4(9)	6354(2)	1408.9(14)	25.0(4)
O16	2020.4(9)	3743(2)	1301.5(14)	31.5(4)
O17	1862.5(8)	5960(2)	2922.6(14)	25.5(4)
O18	1204.3(8)	6283(2)	4781.5(14)	23.8(4)

[a] U_{eq} is defined as 1/3 of the trace of the orthogonalized U_{ij} tensor.

dx.doi.org/10.1021/ic500331u | Inorg. Chem. 2014, 53, 6034−6041

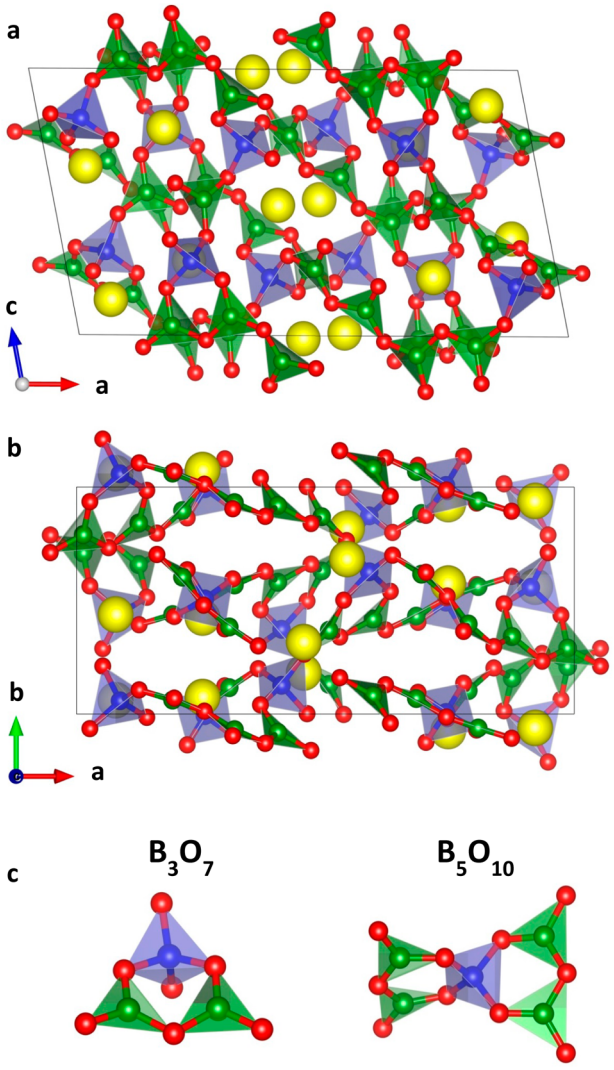

Figure 4. Structure of $Li_3B_{11}O_{18}$, viewed along (a) [010] and (b) [001]. (c) View of the B_3O_7 and B_5O_{10} groups present as building entities in the structure of $Li_3B_{11}O_{18}$. O and Li atoms are colored red and yellow, respectively; BO_3 triangular units are colored green, while BO_4 tetrahedra are colored blue.

Interestingly, these B_3O_7 (2Δ+T) and B_5O_{10} (4Δ+T) groups are also observed as building units in borates of similar composition, i.e., in the $M_2O-nB_2O_3$ family, where M = Na,[30] K,[31] Rb,[32] Cs,[33] and Ag,[34] and with n close to 4. However, as the exact composition varies from one to another, these blocks are connected in different ways, demonstrating the extraordinary richness of the crystalline structures in this system.

Lithium atoms are distributed among three crystallographic sites, and they are four-coordinated with Li−O distances ranging from 1.9 to 2.2 Å—with in addition a few longer Li−O bonds up to 2.60 Å—in perfect agreement with what is usually observed in other Li-based oxides (Supporting Information, Figure S2). A bond valence sum analysis performed in the same way as explained above for $Li_6B_4O_9$ also confirms the validity of the structure (see the Supporting Information, Table S4).

Our structural determination retrospectively explains why neither Bétourné et al.[11] nor Mathews et al.[25] could solve the structure: the former study considered a wrong composition, and they suffered from poor quality of their single crystals; the latter considered only the powder pattern that likely contained a mixture of $Li_3B_{11}O_{18}$ and boron-rich phase(s) as impurities instead of the expected single-phase $Li_2B_8O_{13}$. Indeed the Rietveld refinement realized on the powder out of which our single crystal was issued presented a few unindexed reflections.

A new synthesis protocol using the right proportion of precursors, i.e., 3:11 instead of 3:12, has been defined in order to obtain powdered $Li_3B_{11}O_{18}$ as a single phase. The same precursors were melted two times at 950 °C for 15 min each and two times at 1050 °C for 5 min each, with intermittent grindings in order to allow a good homogenization of the melt. A first long thermal treatment (5 days) at 550 °C was applied followed by a second thermal treatment at 600 °C for about 24 h. The Rietveld refinement using the structural parameters deduced from single-crystal diffraction is shown in Figure 3; in this case a powder pattern was recorded using the Co Kα radiation, which is suitable for such a large unit cell. The refinement leads to lattice parameters a = 17.7758(2) Å, b = 7.81459(8) Å, c = 9.69032(10) Å, and β = 101.0941(5)° (R_{Bragg} = 2.45%). Overall, this indicates that the $Li_3B_{11}O_{18}$ powder is pure and that the model determined from one single crystal is perfectly valid for the powdered sample.

DISCUSSION

The $Li_2O-B_2O_3$ phase diagram presents a rich crystallochemistry with many compounds corresponding to defined Li_2O:B_2O_3 ratios; the present study has unraveled the two structures that were still undetermined, $Li_6B_4O_9$ and $Li_3B_{11}O_{18}$, which replaces the previously reported $Li_2B_8O_{13}$ composition. Therefore, the vertical line (at 1/4 and shown as a dashed vertical red line in Figure 1) should be slightly shifted toward the Li_2O end-member (new position at 3/11 shown as a plain red line in Figure 1). These two resolved structures ($Li_3B_{11}O_{18}$ and $Li_6B_4O_9$) are of tremendous interest in the understanding of both the glass formation and also the related borate anomalies (T_g, thermal expansion coefficient, ...) observed in alkali borate glasses around the same composition.[3] $Li_3B_{11}O_{18}$ is probably the most interesting crystalline phase in the $Li_2O-B_2O_3$ system since it is constituted by a fully polymerized B_2O_3 network, for which every boron atom is involved in a six-membered ring. These rings could be reminiscent of the boroxol rings (composed of three BO_3 triangles linked by vertices to form planar $B^{[3]}-O-B^{[3]}-O-B^{[3]}-O-B^{[3]}$ rings), which are observed in glassy B_2O_3, and as such, $Li_3B_{11}O_{18}$ could be a good crystalline reference to study borate glasses.

These Li−B−O compounds can be successfully examined through the dimensional reduction formalism developed by Tulski and Long[35] for solid structures. Dimensional reduction describes how the metal−anion (M−X) framework of a parent compound, MX_x, is dismantled upon reaction with an ionic reagent A_aX to form a child compound $A_{na}MX_{x+n}$, according to the reaction

$$MX_x + nA_aX \rightarrow A_{na}MX_{x+n} \quad (1)$$

Binary parent; ternary child; dimensional reduction agent

The anions X (here oxygen) may serve as either bridging or terminal ligands on the metal centers M, and the added equivalents are incorporated into the M−X framework. The charge-balancing counterions A are much more electropositive than M and will not form strong covalent bonds with the

dx.doi.org/10.1021/ic500331u | Inorg. Chem. 2014, 53, 6034−6041

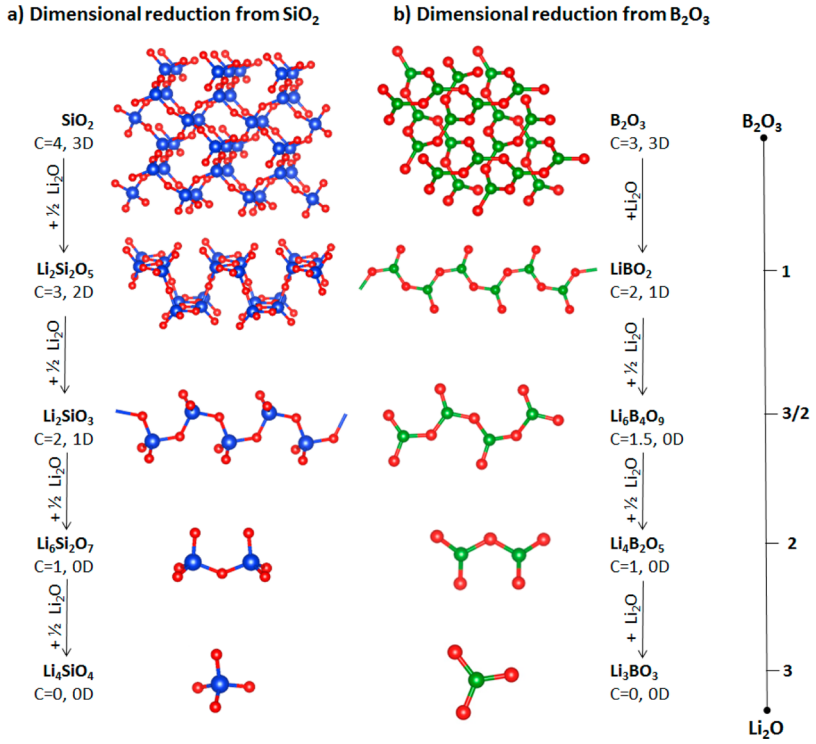

Figure 5. Dimensional reduction formalism when n Li_2O is incorporated in the parent SiO_2 structure (a) or in the parent B_2O_3 structure (b) to form $Li_{2n}SiO_{2+n}$ and $Li_{2n}B_2O_{3+n}$ compounds, respectively. The figure for (a) is inspired from ref 35. For $Li_{2n}B_2O_{3+n}$, only compositions with BO_3 triangular units are considered. The structures are shown only through their Si−O or B−O framework (Li atoms are omitted for clarity). The values on the right scale give the relative Li_2O versus B_2O_3 ratio in the binary phase diagram. The connectedness C decreases with increasing the Li_2O content, and simultaneously the dimension of the structures decreases from 3D to 0D.

anions. The M coordination geometry and the mode of connectivity (i.e., whether neighboring coordination polyhedra share corners, edges, or faces) should remain constant under this reaction. One may also note that the M oxidation state should not be modified by incorporation of A. This phenomenological approach was successfully tested in many solid structures and is also a mean to guess the structure of a child compound when incorporating A_aX in a parent compound. The dimensional reduction approach was shown to be highly reliable when A is a small and polarizing cation (A highly electropositive); therefore Li is a perfect candidate.

A nice illustration[35] of dimensional reduction can be seen in the successive structures adopted when Li_2O is incorporated in a SiO_2 covalent parent framework (Figure 5), following the reaction

$$SiO_2 + nLi_2O \rightarrow Li_{2n}SiO_{2+n} \quad (2)$$

From SiO_2 to Li_4SiO_4, the 3D structure made of corner-sharing SiO_4 tetrahedra is sequentially modified, while Li deconstructs the framework so as to obtain layers ($Li_2Si_2O_5$), then chains (Li_2SiO_3), and clusters made of two SiO_4 ($Li_6Si_2O_7$), to end up with a fully saturated framework made of isolated SiO_4 tetrahedra surrounded by Li in the end-member Li_4SiO_4. A useful indicator regarding this series of mother/child reactions is the *connectedness* of a structure, which is calculated by summing the number of linkages extending from a center M*i* through all CN_{Mi} of its coordinated anions X*j* and then averaging the sums obtained for each of the m different metal centers in a repeat unit:

$$\text{connectedness} = \frac{1}{m}\sum_{i=1}^{m}\sum_{j=1}^{CN_{Mi}}(CN_{Xj} - 1) \quad (3)$$

In the above formula, CN_{Xj} denotes the number of M atoms coordinated to the anions X*j*. The connectedness can be simplified to

$$\text{connectedness} = 2 \times [CN_M - (x + n)] \quad (4)$$

in the case of a child compound $A_{na}MX_{x+n}$ featuring only one- and two-coordinated anions ($CN_X \in \{1,2\}$).

The connectedness of the Li_nSiO_{x+n} child compounds decreases step by step from four to zero during the parent−child sequences shown in Figure 5a; therefore this important parameter was proposed by Tulski and Long as a means to quantify the dimensional reduction in any MX_x structure.

The Li−B−O system perfectly fits in line with this formalism, since the B−O framework consists of rigid covalent B−O bonds, and Li is a highly electropositive cation as mentioned before. It was therefore tempting to apply it to the crystalline phases reported in the Li_2O−B_2O_3 phase diagram; this was to our knowledge never done before. Indeed, boron-based compounds were not included among the 3000 crystal structures considered for establishing the dimensional reduction formalism.[35] The reason most likely lies in the versatility in the coordination polyhedron around boron atoms: contrary to Si, S, or P, which most likely adopt a tetrahedral coordination with oxygen atoms, boron can form equally either BO_3 triangles or BO_4 tetrahedra, both being sometimes observed in the same compound as exemplified by $Li_3B_{11}O_{18}$.

dx.doi.org/10.1021/ic500331u | Inorg. Chem. 2014, 53, 6034−6041

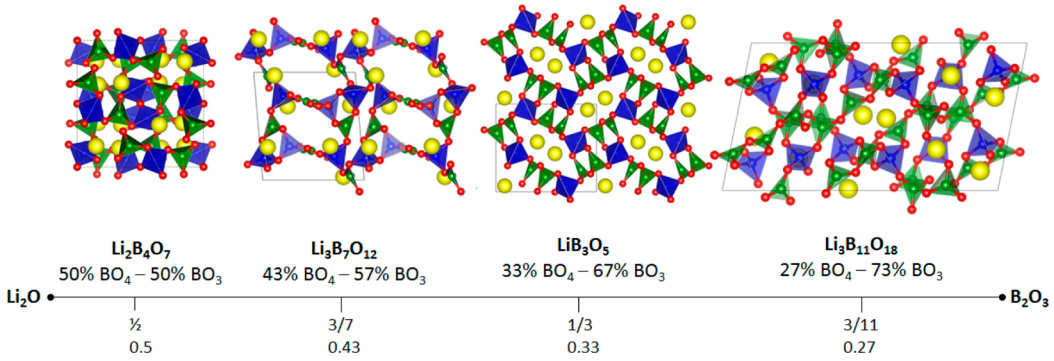

Figure 6. Portion of the $Li_2O-B_2O_3$ phase diagram between 0.27 and 0.5 (Li_2O versus B_2O_3 ratio), highlighting the relative amount of BO_4 tetrahedra (blue) versus BO_3 triangular units (green). Li is yellow.

A dimensional reduction formalism was therefore considered to examine the gradual insertion of Li_2O into parent B_2O_3, following the equation

$$B_2O_3 + nLi_2O \rightarrow Li_{2n}B_2O_{3+n} \quad (5)$$

To circumvent the problem of versatility in boron coordination, only compounds solely built on BO_3 triangular units were considered. Their B–O framework and their connectedness (C) are reported in Figure 5b. The parent B_2O_3 compound is built on a tridimensional (3D) network of corner-shared BO_3 triangles; its connectedness is calculated to be 3. On inserting Li_2O, the child compound $LiBO_2$ ($Li_2O-B_2O_3$) presents infinite chains of corner-shared BO_3 triangles.[36] The connectedness has then been reduced to 2, and the framework is 1D. Further insertion of 1/2 Li_2O leads to $Li_6B_4O_9$ (3 Li_2O–2 B_2O_3); additional Li have broken the infinite chain (1D) into clusters (0D) made of four BO_3 units (B_4O_9 groups), with a connectedness of 1.5. The latter is then reduced to 1 while another 1/2 Li_2O inserted; this corresponds to the breaking of the B_4O_9 clusters made of four BO_3 in two diborate groups as reported recently in the α- and β-polymorphs of $Li_4B_2O_5$ (2 $Li_2O-B_2O_3$).[14] At this stage, incorporation of Li_2O fully saturates the B–O framework as the BO_3 groups get isolated; the connectedness decreases to zero in Li_3BO_3 (3 $Li_2O-B_2O_3$).[37] Therefore, one can notice that there is an almost perfect parallelism between dimensional reduction from parents SiO_2 and B_2O_3, the main difference lying in the structural unit, which is a tetrahedron for the former, while a triangular unit for the latter.

As explained above, the specificity of boron is to be able to form two different coordination polyhedra; for example boron is seen only in the middle of BO_4 tetrahedra in the high-pressure polymorph of $LiBO_2$,[38] while the ambient pressure form contains solely BO_3 groups. There are also several compounds that present both BO_3 and BO_4 groups: in addition to $Li_3B_{11}O_{18}$ reported here, one may cite LiB_3O_5[8] (and also its high-pressure polymorph[6]), $Li_3B_7O_{12}$,[39] and $Li_2B_4O_7$.[31] As can be seen from Figure 6, these compounds are located in a small part of the binary phase diagram, with Li_2O:B_2O_3 ratios ranging from 0.27 ($Li_3B_{11}O_{18}$) to 0.5 ($Li_2B_4O_7$). Coincidentally or not, the solubility of these compounds is here at a minimum.[25] From $Li_3B_{11}O_{18}$ to $Li_2B_4O_7$, the relative proportion of BO_4 units increases regularly from 27% to 50% while increasing the Li_2O content in the formulas. For Li_2O:B_2O_3 ratio greater than 0.5, lithium borate compounds comprise only BO_3 triangular units.

To conclude, the insertion of Li_2O in the parent B_2O_3 compound occurs with two competitive processes. First, the relative amount of BO_3 triangle units tends to lower with the benefit of BO_4 tetrahedral units, where a maximum is found at 1:2 ratio (composition $Li_2B_4O_7$, for which an equal number of BO_3 and BO_4 is obtained). This is linked to a densification of the compound, and this can be explained by a pressure effect (for instance, one may remember that the high pressure form of B_2O_3 is built from BO_4 groups only[38]). Increasing further the amount of Li_2O provokes a drastic change in the structural behavior, as compounds switch back to 100% BO_3 units, with a behavior that perfectly fits in line with the dimensional reduction formalism.

CONCLUSION

In this paper, the crystal structure determination of two lithium borates is reported: $Li_6B_4O_9$ and $Li_3B_{11}O_{18}$. The latter compound demands a reinterpretation of the $Li_2O-B_2O_3$ phase diagram, as it proves that the composition $Li_2B_8O_{13}$ does not exist. Both $Li_6B_4O_9$ and $Li_3B_{11}O_{18}$ compounds crystallize with monoclinic symmetry, and the main difference between them lies in the coordination of boron. $Li_6B_4O_9$ presents solely BO_3 triangular units, and its connectedness of 1.5 is in perfect line with the dimension reduction formalism. The structure of $Li_3B_{11}O_{18}$ is more complex, as it is built upon a 3D framework of BO_3 triangular units and BO_4 tetrahedra linked through vertices.

ASSOCIATED CONTENT

Supporting Information

The crystal data, Li environments, bond valence sum analysis, and CIF files of $Li_6B_4O_9$ (icsd code 427421) and $Li_3B_{11}O_{18}$ (icsd code 427426) are available as supporting materials. This material is available free of charge via the Internet at http://pubs.acs.org.

AUTHOR INFORMATION

Corresponding Authors

*E-mail: gwenaelle.rousse@upmc.fr.
*E-mail: gerald.lelong@impmc.upmc.fr.

Notes

The authors declare no competing financial interest.

ACKNOWLEDGMENTS

The authors would like to thank Drs. G. Ferlat, G. Radtke, and L. Cormier for fruitful discussions.

REFERENCES

(1) Sastry, B. S. R.; Hummel, F. A. *J. Am. Ceram. Soc.* **1958**, *41*, 7−17.
(2) Sastry, B. S. R.; Hummel, F. A. *J. Am. Ceram. Soc.* **1959**, *42*, 216−218.
(3) Wright, A. C. *Phys. Chem. Glasses: Eur. J. Glass Sci. Technol., Part B* **2010**, *51*, 1−39.
(4) Ferlat, G.; Seitsonen, A. P.; Lazzeri, M.; Mauri, F. *Nat. Mater.* **2012**, *11*, 925−929.
(5) Touboul, M.; Penin, N.; Nowogrocki, G. *Solid State Sci.* **2003**, *5*, 1327−1342.
(6) Neumair, S. C.; Vanicek, S.; Kaindl, R.; Többens, D. M.; Wurst, K.; Huppertz, H. *J. Solid State Chem.* **2011**, *184*, 2490−2497.
(7) Heller, G. In *Structural Chemistry of Boron and Silicon; Topics in Current Chemistry*; Springer: Berlin, 1986; pp 39−98.
(8) König, H.; Hoppe, R. *Z. Anorg. Allg. Chem.* **1978**, *439*, 71−79.
(9) Becker, P. *Adv. Mater.* **1998**, *10*, 979−992.
(10) Ohta, S.; Komagata, S.; Seki, J.; Saeki, T.; Morishita, S.; Asaoka, T. *J. Power Sources* **2013**, *238*, 53−56.
(11) Bétourné, E.; Touboul, M. *J. Alloys Compd.* **1997**, *255*, 91−97.
(12) Bétourné, E.; Touboul, M. *Powder Diffr.* **1997**, *12*, 155−159.
(13) Yamada, A.; Iwane, N.; Harada, Y.; Nishimura, S.; Koyama, Y.; Tanaka, I. *Adv. Mater.* **2010**, *22*, 3583−3587.
(14) He, M.; Okudera, H.; Simon, A.; Köhler, J.; Jin, S.; Chen, X. *J. Solid State Chem.* **2013**, *197*, 466−470.
(15) Tao, L.; Neilson, J. R.; Melot, B. C.; McQueen, T. M.; Masquelier, C.; Rousse, G. *Inorg. Chem.* **2013**, *52*, 11966−11974.
(16) Tao, L.; Rousse, G.; Chotard, J. N.; Dupont, L.; Bruyère, S.; Hanžel, D.; Mali, G.; Dominko, R.; Levasseur, S.; Masquelier, C. *J. Mater. Chem. A* **2014**, *2*, 2060−2070.
(17) Senyshyn, A.; Boysen, H.; Niewa, R.; Banys, J.; Kinka, M.; Burak, Y.; Adamiv, V.; Izumi, F.; Chumak, I.; Fuess, H. *J. Phys. Appl. Phys.* **2012**, *45*, 175305.
(18) Clark, R. C.; Reid, J. S. *Acta Crystallogr. A* **1995**, *51*, 887−897.
(19) *CrysAlis PRO*, version 171.37.31; Agilent Technologies Ltd: Yarnton, England, 2014.
(20) Dolomanov, O. V.; Bourhis, L. J.; Gildea, R. J.; Howard, J. A.; Puschmann, H. *J. Appl. Crystallogr.* **2009**, *42*, 339−341.
(21) Sheldrick, G. M. *Acta Crystallogr. A* **2008**, *64*, 112−122.
(22) Rietveld, H. M. *J. Appl. Crystallogr.* **1969**, *2*, 65−71.
(23) Rodriguez-Carvajal, J. *Phys. B* **1993**, *192*, 55−69.
(24) Momma, K.; Izumi, F. *J. Appl. Crystallogr.* **2011**, *44*, 1272−1276.
(25) Mathews, M. D.; Tyagi, A. K.; Moorthy, P. N. *Thermochim. Acta* **1998**, *320*, 89−95.
(26) Boultif, A.; Louer, D. *J. Appl. Crystallogr.* **1991**, *24*, 987−993.
(27) Brown, I. D.; Altermatt, D. *Acta Crystallogr. Sect. B: Struct. Sci.* **1985**, *41*, 244−247.
(28) Stephens, P. *J. Appl. Crystallogr.* **1999**, *32*, 281−289.
(29) Mathews, M. D.; Tyagi, A. K.; Moorthy, P. N. *Thermochim. Acta* **1998**, *319*, 113−121.
(30) Penin, N.; Touboul, M.; Nowogrocki, G. *J. Solid State Chem.* **2002**, *168*, 316−321.
(31) Krogh-Moe, J. *Acta Crystallogr. B* **1968**, *24*, 179−181.
(32) Krzhizhanovskaya, M. G.; Bubnova, R. S.; Bannova, I. I.; Filatov, S. K. *Crystallogr. Rep.* **1999**, *44*, 187−192.
(33) Penin, N.; Seguin, L.; Touboul, M.; Nowogrocki, G. *Solid State Sci.* **2002**, *4*, 67−76.
(34) Penin, N.; Touboul, M.; Nowogrocki, G. *Solid State Sci.* **2003**, *5*, 559−564.
(35) Tulsky, E. G.; Long, J. R. *Chem. Mater.* **2001**, *13*, 1149−1166.
(36) Zachariasen, W. H. *Acta Crystallogr.* **1964**, *17*, 749−751.
(37) Stewner, F. *Acta Crystallogr. B* **1971**, *27*, 904−910.
(38) Marezio, M.; Remeika, J. P. *J. Chem. Phys.* **1966**, *44*, 3348−3353.
(39) Jiang, A.; Lei, S.; Huang, Q.; Chen, T.; Ke, D. *Acta Crystallogr. C* **1990**, *46*, 1999−2001.

NOTE ADDED AFTER ASAP PUBLICATION

Due to a production error, the version of this paper that was published ASAP on May 16, 2014, contained errors in Table 1 and the first paragraph of the Discussion section. The corrected version was reposted May 19, 2014.